Research article

NMR IN BIOMEDICINE

Received: 7 January 2012, Revised: 29 August 2012, Accepted: 31 August 2012, Published online in Wiley Online Library: 12 December 2012

(wileyonlinelibrary.com) DOI: 10.1002/nbm.2877

Quantitative comparison of post-processing methods for reduction of frequency modulation sidebands in non-water suppression ^{1}H MRS

Jyh-Miin Lin[a,b], Tzu-Chao Chuang[b], Hsiao-Wen Chung[c] and Shang-Yueh Tsai[d,e]*

Non-water suppression MRS (NWS MRS) has several advantages. First, the unsuppressed water signal can be used as internal calibration for metabolite quantification and as a reliable frequency/phase reference for retrospective motion correction. Second, it avoids the potential artifacts caused by incomplete water suppression (WS) and extra radiofrequency deposition from WS pulses. However, the frequency modulation (FM) sidebands originating from a large water signal will distort the spectrum. Among the methods proposed to solve the problems caused by FM sidebands, post-acquisition processing methods are superior in flexibility for general use compared with experimental methods. In this study, we propose two algorithms based on advanced matrix decomposition to remove the FM sidebands. These methods, the simultaneous diagonalization (QZ) algorithm and its subsequent variant, the simultaneously generalized Schur decomposition (SGSD) algorithm, were numerically evaluated using computer simulations. In addition, we quantitatively compared the performance of these methods and the modulus method in an *in vitro* experiment and *in vivo* NWS MRS against conventional WS data. Our results show that the proposed SGSD algorithm can reduce the FM sidebands to achieve superior estimation of concentration on three major metabolites. This method can be applied directly to spectra pre-acquired under various experimental conditions without modifying the acquisition sequences. Copyright © 2012 John Wiley & Sons, Ltd.

Keywords: MRS and MRSI methods; other spectroscopic methods; artifacts and corrections; post-acquisition processing; non-water suppression; sidebands; frequency modulation; simultaneous diagonalization

INTRODUCTION

For *in vivo* MRS, water suppression (WS) is considered to be a routine procedure to eliminate the large water signals that are three to five orders of magnitude larger than metabolic signals. In clinical MRS, WS is generally performed by applying chemical shift-selective saturation pulses. This requires careful adjustments before each scan. In regions with inhomogeneous fields, such as those surrounding air–tissue interfaces, the performance of WS pulses may decline because of the shift of the resonant frequency of water (1–3). Incomplete WS may lead to a partial saturation effect on nearby metabolites. In addition, the suppression pulse can reduce the spectral quantification accuracy through mechanisms such as the magnetization transfer effect (4) and phase accumulation during motion (5–10). Consequently, the non-water suppression (NWS) MRS technique is an attractive alternative. It not only avoids the aforementioned disadvantages, but also provides several benefits. First, the unsuppressed water signal can be used as internal calibration for metabolite quantification (7,11,12). Second, the unsuppressed water is a reliable frequency/phase reference for retrospective motion correction (2,3,7). Third, compared with WS MRS, NWS MRS has lower radiofrequency (RF) power deposition. In addition, the signal from unsuppressed water can serve as an excellent reference for the calculation of optimally weighted factors required for combining signals from multiple coil elements (13).

NWS MRS is possible using modern 32-bit analog-to-digital converters. Sufficient digital resolution helps to avoid the

* *Correspondence to: S.-Y. Tsai, Graduate Institute of Applied Physics, National Chengchi University, No. 64, Sec. 2, ZhiNan Rd., 11605 Taipei, Taiwan. E-mail: syytsai@gmail.com*

a *J.-M. Lin*
Center for Advanced MR Development, Department of Radiology, Duke University Medical Center, Durham, NC, USA

b *J.-M. Lin, T.-C. Chuang*
Department of Electrical Engineering, National Sun Yat-sen University, Kaohsiung, Taiwan

c *H.-W. Chung*
Department of Electrical Engineering, National Taiwan University, Taipei, Taiwan

d *S.-Y. Tsai*
Graduate Institute of Applied Physics, National Chengchi University, Taipei, Taiwan

e *S.-Y. Tsai*
Research Center for Mind, Brain and Learning, National Chengchi University, Taipei, Taiwan

Abbreviations used: *Cre, creatine; CRLB, Cramer–Rao lower bound; FID, free induction decay; FM, frequency modulation; GEP, generalized eigenproblem; Gln, glutamine; Glu, glutamate; Glx, Glu + Gln; mI, myo-inositol; NAA, N-acetylaspartate; NEX, number of excitations; NWS, non-water suppression; PRESS, point-resolved spectroscopy; QZ, simultaneous diagonalization; RF, radiofrequency; SGSD, simultaneously generalized Schur decomposition; SNR, signal-to-noise ratio; SVD, singular value decomposition; tCho, total choline; WS, water suppression.*

NMR IN BIOMEDICINE

problems caused by quantization errors (14). Therefore, the extraction of a large water component from the NWS spectra can be conducted accurately using post-processing algorithms (14–16). In this manner, the quantification of metabolites using NWS MRS is feasible (17). However, the large water peak causes another considerable problem in NWS MRS, especially for spectra acquired at short TE. The frequency modulation (FM) sidebands located at bilateral sides of the spectra can impose noticeable lineshape distortion on the spectra (18). Using spatial localization and spoiler gradients in the MRS scan, the phase of the received signal is altered according to the mechanical oscillations at acoustic frequencies. The induced temporary phase oscillation, modeled as FM, creates sidebands on the spectrum with magnitudes that are usually at small fractions of the signal. The intensity and phases of these parasitic sideband artifacts are determined by three major factors: the intensity of the signal, TE and the position in the scanner. Because the water signal is approximately 10^3–10^5 times larger than the signals of metabolites in NWS MRS (14), the magnitude of FM sidebands from water signals is approximately the same order as the signals of the metabolites (19). These FM sideband artifacts may superimpose on the spectral region in which the metabolites of interest reside, leading to an erroneous estimation of the concentration.

In general, FM sidebands are induced by spoiler gradients (4). Several experimental methods have been proposed to deal with FM sidebands in NWS MRS. The most intuitive method to avoid FM sidebands is to alternate the phase of spoiler gradients. One experimental method inverted the phases of spoiler gradients in sequential scans and subsequently combined them to cancel all FM-related components (20). However, potential motion artifacts may cause phase variation (7,15), which can lead to various phases and intensities of FM sidebands. Therefore, it is difficult to achieve total cancellation of FM sidebands through gradient phase alternation in the presence of subject motion. Similarly, phase correction according to an additional reference scan on extraneous phantoms (12) usually cannot fully retain the phase variation, because the locations and scanning environments are usually inconsistent between phantom and *in vivo* experiments. Another experimental approach used oversampled *J*-resolved experiments. Multiple MRS scans with various TEs were performed to obtain two-dimensional spectral data. The FM sidebands were off-set in every frame of two-dimensional spectra and could be removed (21). However, the total scan time of this method was prolonged and the spectra were heavily weighted by the long TE signal. Compared with experimental methods, post-acquisition processing methods are appealing substitutes because they do not require any substantial change in hardware or pulse sequence. A post-processing method, also called the modulus method, has been proposed to eliminate the FM sidebands by direct use of the magnitude part of the free induction decay (FID), that is, the modulus signal (22). However, the main disadvantage of the modulus method is the signal-to-noise ratio (SNR) reduction, which is theoretically achieved by a factor of the square root of two (20). In addition, the magnitude part of the signal may alter the spectral shape.

This study aimed to develop novel post-processing methods using two advanced algebraic algorithms for the reduction of FM sidebands in NWS MRS, and to quantitatively compare the performance of various post-processing methods. The novel post-processing methods were devised with the simultaneous diagonalization (QZ) algorithm and the simultaneously generalized Schur decomposition (SGSD) algorithm to solve for eigenvalues and eigenvectors. The SGSD algorithm is expected to consistently decompose multiple matrices (more than two) simultaneously, thereby fostering numerical stability. Computer simulations were performed to evaluate the performance of the proposed methods. Quantitative comparisons were conducted among various post-processing methods for data that were acquired either *in vitro* or *in vivo*.

THEORY

The property of FM sidebands in FID

The FM sidebands can be expressed as multiple pairs of symmetrical sidebands with opposite phases. The FID of the water signal can be expressed by the following formula (19):

$$\begin{aligned} s_{water}(t) &= Ae^{-t/T2*}e^{i[\omega_c t + m_f \sin(\omega_G t)]} \\ &= Ae^{-t/T2*}J_0(m_f)e^{i(\omega_c t)} + Ae^{-t/T2*}\sum_{n=1}^{\infty}(-1)^n J_n(m_f) \\ &\quad \left[e^{i(\omega_c - n\omega_G)t} + (-1)^n e^{i(\omega_c - n\omega_G)t}\right] \end{aligned} \quad [1]$$

where A is the amplitude of water and m_f is the modulation index that is mainly contributed by spoiling gradients. The contribution from slice-selective gradients can be negligible (18). ω_c is the water frequency (the carrier) and ω_G is the modulating frequency. In Equation [1], the signal is expressed as the combination of the main water peak (first term in Equation [1]) located at the center of the spectrum and numerous harmonic signals present as sidebands on the spectrum. The coefficients of successive terms are the Bessel functions for nth-order harmonics, $J_n(m_f)$. Because m_f is small, the higher order Bessel function ($n > 1$) can be approximated to zero. For example, the second-order Bessel function $J_2(5 \times 10^{-6}) = 3.1 \times 10^{-12}$. Therefore, we can apply narrow-band approximation to the FM part. FM sidebands can be separated from the water signal as:

$$\begin{aligned} s_{FM}(t) &\approx -Ae^{-t/T2*}J_1(m_f)\left[e^{-i\omega_m t} - e^{i\omega_m t}\right] \\ &\approx -2i{\cdot}Ae^{-t/T2*}J_1(m_f)\sin(-\omega_m t)\} \end{aligned} \quad [2]$$

where ω_m represents $\omega_c - \omega_G$. Because the main water signal is located around the center of the spectrum, ω_c can be assumed to be zero and ω_m is equal to $-\omega_G$. In summary, the FID, including signals from water, metabolites and FM sidebands, can be expressed as:

$$\hat{s}(t) = s(t) + s_{FM}(t) \approx s(t) + 2i{\cdot}Ae^{-t/T2*}J_1(m_f)\sin(-\omega_m t) \quad [3]$$

where $s(t)$ represents the summation of water and metabolites without FM sidebands. Thus, our goal is to differentiate $s(t)$ from $s_{FM}(t)$.

According to Equation [3], the signals of FM sidebands have only an imaginary part. Therefore, the first step in our method is to modify the weighting of real and imaginary parts through a factor Δ. In this manner, the real part is increased by the factor $(1 + \Delta)$, whereas the imaginary part is attenuated by the factor $(1 - \Delta)$, yielding:

$$\begin{aligned} \hat{s}_\Delta(t) &= (1+\Delta)\mathrm{Re}\{\hat{s}(t)\} + (1-\Delta)i{\cdot}\mathrm{Im}\{\hat{s}(t)\} \\ &= (1+\Delta)\mathrm{Re}\{s(t)\} + (1-\Delta)i{\cdot}\mathrm{Im}\{s(t)\} + (1-\Delta)i{\cdot}\mathrm{Im}\{s_{FM}(t)\} \\ &= s(t) + \Delta{\cdot}s(t) + (1-\Delta)s_{FM}(t) \end{aligned} \quad [4]$$

The alterations of the signal as a function of Δ can be separated into three parts. First, $s(t)$ remains unchanged regardless of Δ; second, the complex conjugated part of $s(t)$ is increased by Δ and mirroring peaks will show up according to increasing variation of Δ; third, the FM sidebands $s_{FM}(t)$ are reduced by a weighting factor (1 – Δ), and can be completely eliminated when Δ = 1. Specifically, by tracking the alterations of amplitudes *versus* Δ, these two parts (the conjugate part and FM sidebands) can be differentiated. In this manner, the behavior of each term is predictable and the amplitudes of FM sidebands will vary in a direction opposite to factor Δ. This enables us to track the alteration of each spectral peak at various Δ. Once the signal alteration opposite to Δ is found, we can extract and remove the FM sidebands.

To extract FM sidebands, we used a time-domain approach to obtain the potential resonances on the spectrum, also known as poles. In brief, we incorporated signals from Equation [4] into the generalized eigenproblem (GEP). Subsequently, we used the extended QZ algorithm and SGSD algorithm to solve GEP by simultaneous triangularization (23–26). The whole procedure of SGSD is shown in Figure 1, the principles of which are presented in the following section.

Generalized eigenproblem

In general time-domain approaches, the FID signal is assumed to be a linear combination of multiple decaying sinusoids. Therefore, these unknown sinusoids can be retrieved with properly arranged data matrices. In essence, the complex amplitudes of the signal are formulated using the following equation:

$$y(t) = \sum_{i}^{k} A_i \lambda_i{}^t + e(t) \qquad [5]$$

The complex pole λ_i represents the rotating rate (chemical shift), including the T_2* effect. The complex amplitude A_i represents the magnitude and phase of each pole. $e(t)$ are white noises.

Each decaying sinusoid represents a spectral resonance belonging to either a certain metabolite or water. Numerous algorithms have been developed to obtain poles and corresponding amplitudes from this basic linear model by solving for eigenvalues and eigenvectors, such as linear prediction and total least-square linear prediction (27). However, eigen decomposition for a single data matrix usually engenders unstable solutions in the presence of noise. To avoid instability, GEP extends the number of matrices for calculation. In matrix-pencil (28) and filter-diagonalization (29,30) methods, a two-matrix scheme was used to find the common eigenvector. This operation had removed the weak components. These common eigenspaces simplified the solution without prior knowledge of the number of poles, also known as rank. The two-matrix scheme can be further extended to a scheme with three or more matrices. SGSD can be used to decompose them simultaneously with superior stability. The whole process to solve GEP with QZ and SGSD is described in the Appendix.

Utilization of GEP for FM problem

We started the computation by working on two types of time-domain signal, $td_{\_fm}$ (where Δ = 0) and $td_{\_mirror}$ (Δ = 1), where $td_{\_mirror}$ is immune to FM sidebands, but has mirror peaks from the lower field range. These two time-domain signals were used to construct data matrices U_{0_fm}, U_{1_fm},... and U_{0_mirror}, U_{1_mirror},... according to Equations [A1] and [A2]. Subsequently, all matrices were simultaneously triangularized by QZ and SGSD:

$$\begin{matrix} U_{rt_{fm}} = QU_{r_{fm}}Z, \\ U_{rt_{mirror}} = QU_{r_{mirror}}Z \end{matrix} \quad r = 0,\ 1, \ldots R \qquad [6]$$

where r is the starting time point of the time-domain signal used to generate the U matrices, and was assigned as 0 or 1 because a larger number prolongs the computation time by including more matrices. QZ only decomposes two matrices, which indicates that the entire set of matrices has been quasi-triangularized. SGSD can process the entire set of matrices.

After being triangularized, the diagonal elements of U_{0t_fm} and U_{1t_fm} and their corresponding eigenvectors were used to estimate the preliminary parameters of the poles λ_i and the initial amplitudes A_i according to Equations [A6] and [A7]. In addition, we retrieved the parameter α_i from the ratio of diagonal elements of U_{rt_mirror} and U_{rt_fm}, which is related to the variation of FM sidebands regarding Δ (i.e. the 'slope' of the variation). The final step is to correct for the initial amplitude (A_i) through α_i according to Equation [7]. Those with $|\alpha_i| \geq 1$, exceeding the expected trend, are unrelated to FM; therefore, their original values were preserved. That is:

$$\hat{A}_i = \begin{cases} A_i, for |\alpha_i| \geq 1 \\ \dfrac{\Delta + \alpha_i - 1}{\Delta} \cdot A_i, |\alpha_i| < 1 \end{cases} \qquad [7]$$

The poles λ_i are preserved because they represent the rotation (resonance frequency) and decay rate (relaxation).

Consideration for errors

To evaluate the stability of the solution in Equation [7] under the perturbation of noise, we calculated the Cramer–Rao lower bound (CRLB). The CRLB provides the minimal achievable variance accompanying the unbiased estimator. The deduction of CRLB based on the time-domain model has been described in a previous report (31). In brief, it is the incorporation of factor Δ-imposed nonlinear behavior to the estimation of the parameters. For example, according to Equation [4], the Gaussian

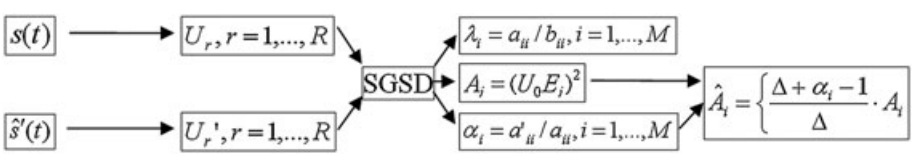

Figure 1. Block diagram for removing frequency modulation (FM) sidebands using the simultaneously generalized Schur decomposition (SGSD) algorithm.

NMR IN BIOMEDICINE

white noise increased by a factor of $(1+\Delta^2)$ because we modified both the real part (increasing by Δ) and the imaginary part (decreasing by Δ). Furthermore, the CRLB in Equation [7] can be calculated by combining the Jacobian, which is also related to Δ:

$$CRLB_{\alpha} = \left[\frac{\partial\alpha}{\partial A'}, \frac{\partial\alpha}{\partial A}\right] \times CRLB_{A',A} \times \left[\frac{\partial\alpha}{\partial A'}, \frac{\partial\alpha}{\partial A}\right]^{T} \quad [8]$$

The CRLB of the corrected amplitudes can be generated as:

$$CRLB_{\hat{A}} = \frac{1}{\Delta^2 A^2}[1, -1+\Delta] \times CRLB_{A',A} \times [1, -1+\Delta]^{T} \quad [9]$$

The diagonal elements of the middle terms represent the CRLB of A′ and A. However, because the off-diagonal elements of the covariance matrices were unknown, a reasonable upper bound of the off-diagonal covariance was derived by:

$$CRLB_{A',A}(1,2) = CRLB_{A',A}(2,1) < \sqrt{CRLB_{A',A}(1,1) \times CRLB_{A',A}(2,2)} \quad [10]$$

This indicates that the lower bound in Equation [9] can be treated as an approximation of CRLB. The assumption for the deduction is that the linearity is valid within a narrow region. This occurs when the noise is sufficiently small.

METHODS

Computer simulations

Monte Carlo simulations were performed to compare the numerical performance of QZ and SGSD. Three poles with a damped factor of 0.01 (i.e. $T_2^* = 10$ ms) were simulated as three metabolites. The frequencies of these metabolites were −50, −100 and −150 Hz. Additional peaks were simulated symmetrically around the center with opposite phases to the FM sidebands. The frequencies were 200 and −200 Hz. Only first-order FM sidebands were simulated because the higher order terms were small. The biases and variances of the estimator in Equation [7] were evaluated at various noise levels with data lengths of 32 and 128. The CRLB was calculated from Equation [10]. All simulations were performed using MATLAB software (MathWorks, Natick, MA, USA). Simulations were repeated 500 times. SNR was defined in units of decibel as the signal power over noise variances:

$$SNR \stackrel{def}{\equiv} 10 \times Log_{10}\left(\frac{A^2}{\sigma^2}\right) \quad [11]$$

In vivo and *in vitro* experiments

Experiments on human participants and a spectroscopy phantom were performed using a 3-T MRI scanner (Trio, Siemens Medical Solutions, Erlangen, Germany) with an eight-channel coil array. For *in vivo* experiments, 11 healthy subjects were enrolled in this study under informed consent. The single-voxel point-resolved spectroscopy (PRESS) sequence was used to acquire MRS data from a selected volume ($20 \times 20 \times 20$ mm^3) located at the parietal lobe in the brain (Fig. 2) with the following experimental parameters: TE = 30 ms; TR = 2000 ms; number of excitations (NEX), 128; dummy scan, 2; bandwidth, 2000 Hz; spectral points, 2048. In the PRESS sequence, we used sinc-type RF pulses with a duration of 2.6 ms for excitation and refocusing. Two sets of spoiler gradients were incorporated around the two refocusing RF pulses. For these two spoiler gradients, the strengths were 7 and 11.5 mT/m in each direction, and the durations were 2 and 4 ms, respectively. NWS and WS scans were collected sequentially for each participant. Shimming and frequency adjustments of the WS pulse were performed carefully to enable the WS MRS data to serve as a standard without influence from FM sideband artifacts. To observe the properties of FM sidebands and evaluate the performance of post-processing methods, additional data were collected from a spectroscopic phantom containing a mixture of metabolite solutions, including 3 mM choline (8), 12 mM creatine (Cre), 18 mM *N*-acetylaspartate (NAA), 7 mM myo-inositol (ml) and 12 mM glutamate (Glu). NWS and WS MRS data were acquired using the single-voxel PRESS sequence with the following experimental parameters: TE = 30 and 80 ms; TR = 2000 ms; volume, $20 \times 20 \times 20$ mm^3; NEX, 256; dummy scan, 2; bandwidth, 2000 Hz; spectral points, 2048.

Once the data had been acquired, FIDs from the eight coils were combined after adjustment for phases and amplitude (32). NWS data were processed using four different procedures for the reduction of FM sidebands, including regular NWS MRS without reduction of FM sidebands, NWS MRS with the QZ algorithm to remove FM sidebands, NWS MRS with the SGSD algorithm to remove FM sidebands and modulus NWS MRS. The process for SGSD and QZ methods focused on the upfield range in which most of the metabolites reside. Subsequently, all MRS data, including NWS and WS data, were transferred into the jMRUI package (java-based Magnetic Resonance User

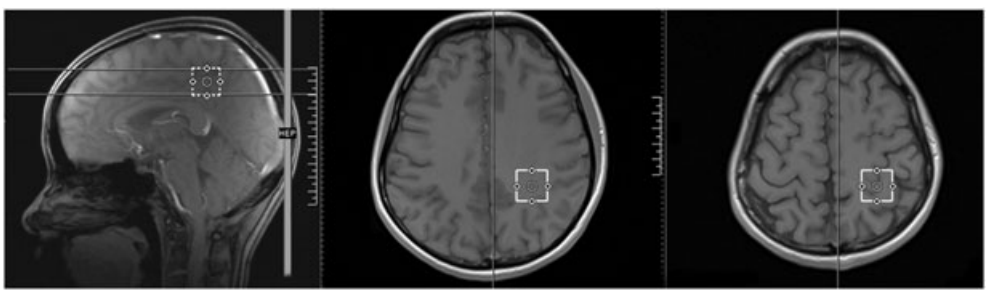

Figure 2. Spatial localization of $20 \times 20 \times 20$-mm^3 volume of interest of the MRS experiment. The volume of interest was defined in the parietal lobe containing mostly white matter (white squares).

Interface, Leuven, Belgium) for spectral processing and analysis. A 5-Hz Lorentzian function was used for apodization. The extraction of water signals for all NWS spectra was performed using the singular value decomposition (SVD)-based algorithm (14) repeatedly to visually flatten the distorted spectra. The frequency shift, damping factor, background distortion and amplitudes of six metabolites, including total choline (tCho), Cre, Glu, glutamine (Gln), mI and NAA, were estimated using the QUEST algorithm (33). The bases of metabolites used for quantification were generated using NMR-Scope simulation with a damping frequency of 13 Hz. Because the modulus of NWS spectra contains only 50% power of the complex signals, the concentrations of the modulus data were adjusted by a factor of two for comparison. The concentrations of NAA, Cre and tCho were compensated for the number of protons (11). To simplify the comparisons, water scaling was conducted without adjustment for water concentrations in various tissues and relaxation effects; therefore, the quantified values were in institutional units (I.U.). The quantified concentrations from the NWS scan with and without FM sideband removal were compared against WS MRS. For phantom experiments, the metabolite concentrations of NAA, Cre and tCho were quantified from NWS data with and without the reduction of FM sidebands. The concentrations were calibrated to absolute concentrations based on those of water (110 M), and were compared with the reference concentrations of the spectroscopy phantom. In addition to absolute concentrations, relative concentrations of NAA/Cre and tCho/Cre were also calculated.

RESULTS

Computer simulations

FM sidebands simulated as the symmetrical peaks around the spectral center can be successfully removed after applying the SGSD algorithm. Figure 3 shows the biases and variance of errors using QZ and SGSD algorithms. Although the performance of SGSD was similar to that of QZ under low SNR, SGSD exhibited less bias and lower variance than QZ at SNR above 20 dB. Furthermore, lower bias and variance were observed with longer data length included in the calculation. Statistically, the minima of variances were provided by CRLB which, as expected, decreased with increasing SNR. The variance of the SGSD algorithm was close to CRLB at all SNR, whereas the variance of QZ was minimized at SNR = 20 dB with no visually discernible improvements at high SNR (Fig. 3C, D).

In vitro experiments

In phantom experiments, we observed the FM sidebands located around 3.3, 1.9, 0.5 and −0.4 ppm on the NWS spectra, and their corresponding anti-phase peaks located on the opposite side of the spectra around the spectral center (Fig. 4A). In addition, FM sidebands were considerably reduced in NWS spectra collected at longer TE (Fig. 4B). Table 1 shows the absolute and relative concentrations estimated from NWS MRS acquired at TE = 30 ms and those after FM sideband reduction by QZ, SGSD and modulus methods. The corresponding errors of the estimated

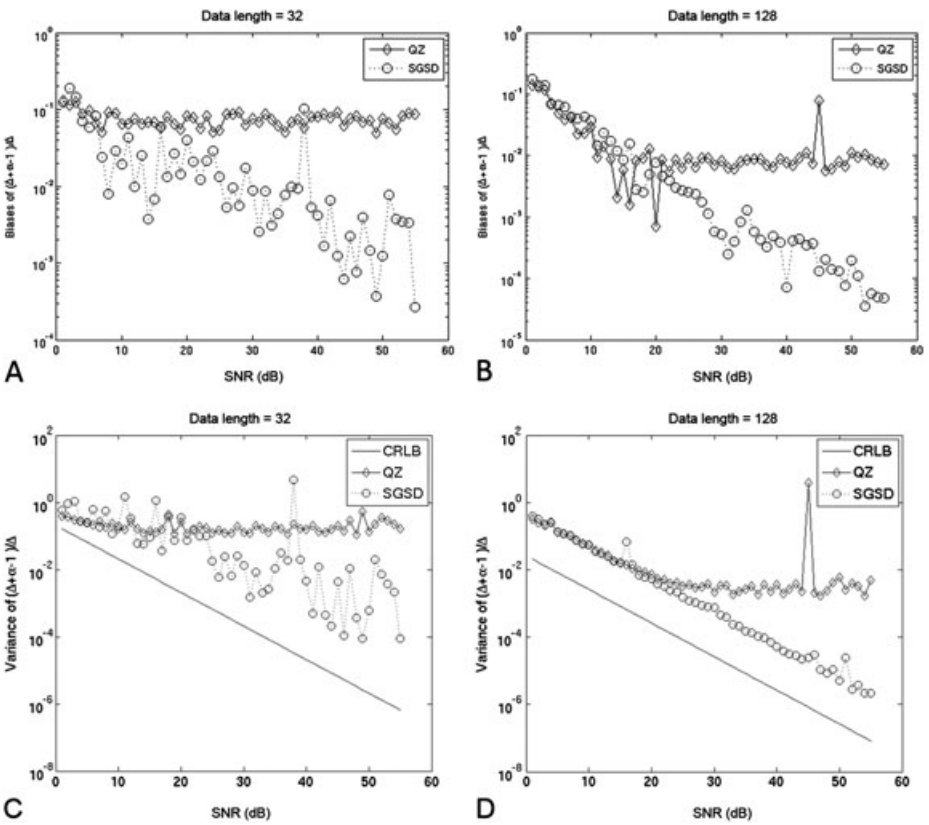

Figure 3. Biases of errors for simultaneous diagonalization (QZ) and simultaneously generalized Schur decomposition (SGSD) algorithms with data lengths of 32 (A) and 128 (B). The SGSD method exhibits a lower error than the QZ method. The large data length improves the accuracy of both methods, which is particularly prominent for QZ at high signal-to-noise ratio (SNR). Variances and Cramer–Rao lower bounds (CRLBs) were estimated using Equation [10] for QZ and SGSD algorithms with data lengths of 32 (C) and 128 (D). The SGSD method exhibits less variance than the QZ method at SNR above 20 dB. A large data length improves the stability of both methods.

NMR IN BIOMEDICINE

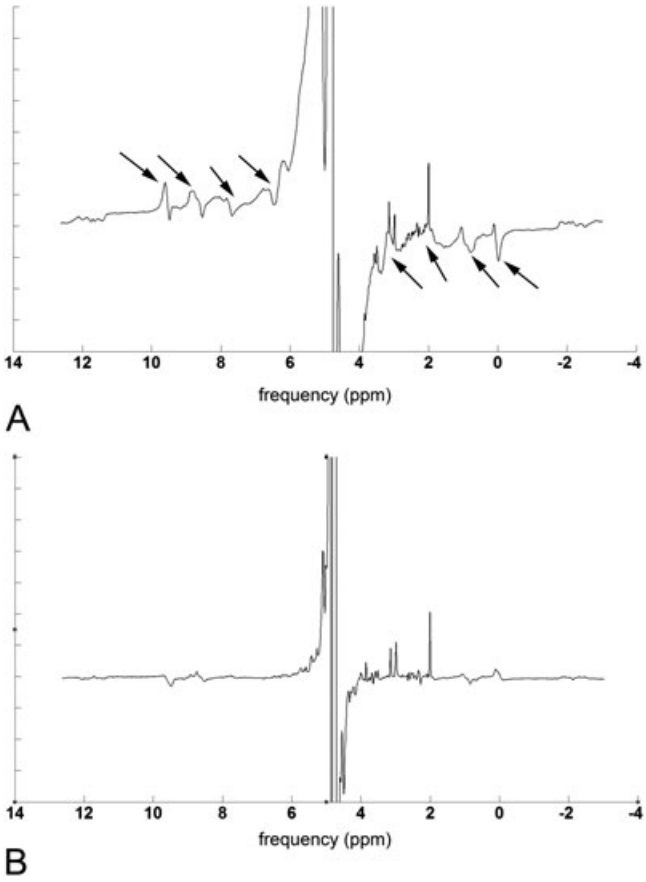

Figure 4. Non-water suppression (NWS) spectra from a phantom experiment collected at TE = 30 ms (A) and TE = 80 ms (B). Frequency modulation (FM) sidebands are presented with anti-phase peaks located symmetrically around the spectral center, as indicated by the arrows. The FM sidebands distort the baseline around the metabolic range, specifically the total choline (tCho) peak around 3.2 ppm. The FM sidebands clearly decrease in amplitude at TE = 80 ms.

concentrations (absolute and relative) were calculated with reference concentrations derived by the spectroscopy phantom. The errors of NAA and Cre were less than 11% with and without reduction of FM sidebands. The SGSD method provides the optimal estimation on Cre (1%) and the modulus method provides the optimal estimation on NAA (3%). The error on tCho was 111% for NWS MRS. After reduction of FM sidebands, errors of tCho decreased to 28%, 11% and 17% for QZ, SGSD and modulus methods, respectively. The relative concentration also exhibited a similar tendency; however, a larger error was observed in NAA/CRE using the QZ method.

In vivo experiments

The difference between the NWS MRS and WS MRS spectra is shown in Figure 5A. FM sidebands in NWS MRS were present around 3.1–3.2 ppm and distorted the spectral baseline around this range. In NWS MRS, the protrusive choline and Cre peaks exhibited overestimated concentrations because of the contamination from FM sidebands. Qualitatively, elevated peaks around 3.2 ppm were observed in NWS spectra and in the difference spectra (Fig. 5A). The elevated peaks were attenuated after correction using the SGSD and QZ algorithms, yielding superior similarity to the WS MRS spectrum (Fig. 5B, C). The flattened difference spectra in the SGSD method, especially around 3.1–3.2 ppm (Fig. 5B), imply that the estimation of FM sidebands is superior using SGSD rather than the QZ method (Fig. 5C).

Figure 6A shows the mean and standard deviation of the concentrations of NAA, tCho and Cre from all subjects. The mean concentrations in NWS spectra were overestimated compared with those in WS spectra. The overestimations in the concentrations were reduced after correction using the QZ, SGSD and modulus methods. For NAA, tCho and Cre on the 11 participants, the metabolite concentrations measured from spectra with FM sidebands corrected using the SGSD method exhibited the optimal estimation with the smallest percentage errors, as shown in Figure 6B. In addition, we quantified mI, Glu and Gln, which were composed of several multiplets. All three correction methods included in this study failed to retain the spectral shapes.

DISCUSSION

In this study, we have developed novel post-acquisition processing methods to reduce FM sidebands in NWS MRS, and have compared quantitatively the performance of the three methods in both *in vivo* and *in vitro* experiments. The proposed methods

Table 1. Absolute and relative concentrations of *N*-acetylaspartate (NAA), total choline (tCho) and creatine (Cre) from *in vitro* MRS data collected at TE = 30 ms

Concentration (mM)	Reference	NWS	NWS QZ	NWS SGSD	NWS modulus
NAA	18	20.02	19.88	19.57	17.54
Cre	12	12.99	10.86	11.85	11.11
tCho	3	6.34	3.83	3.34	2.50
NAA/Cre	1.5	1.54	1.83	1.65	1.59
tCho/Cre	0.75	1.46	1.06	0.84	0.68
Errors (%)					
NAA	–	11	10	9	3
Cre	–	8	9	1	7
tCho	–	111	28	11	17
NAA/Cre	–	3	22	10	5
tCho/Cre	–	95	41	13	10

NWS, non-water suppression; QZ, simultaneous diagonalization; SGSD, simultaneously generalized Schur decomposition.

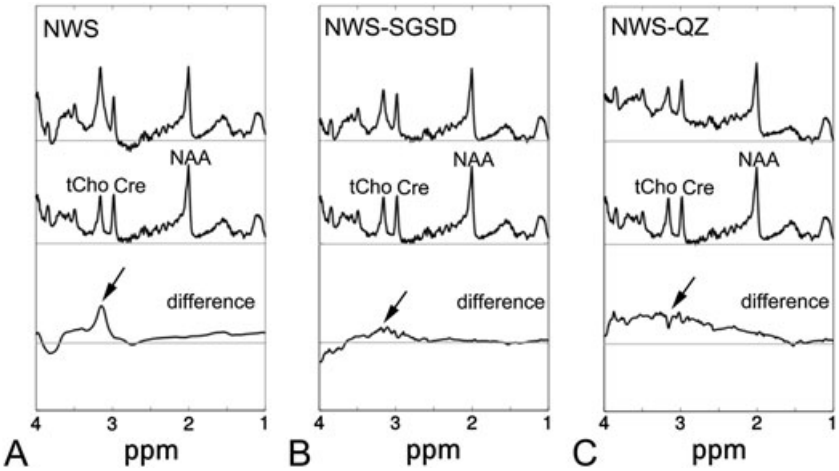

Figure 5. Representative *in vivo* spectra of non-water suppression (NWS) MRS (A), NWS MRS after simultaneously generalized Schur decomposition (SGSD) correction (B) and NWS MRS after simultaneous diagonalization (QZ) correction (C). Spectra of water suppression (WS) MRS and difference spectra between NWS and WS MRS are shown in the middle and bottom of each plot. An elevated choline peak can be observed on the NWS MRS spectrum (A). After correction, its level is close to that of the WS MRS spectrum (B, C). The effect of frequency modulation (FM) sidebands on the choline peak can be observed on the difference spectra (black arrows). SGSD exhibits superior estimation on FM sidebands, yielding flattened difference spectra (B). By contrast, a small negative peak around 3.2 ppm can be observed on the difference spectra of the QZ method (C). Cre, creatine; NAA, *N*-acetylaspartate; tCho, total choline.

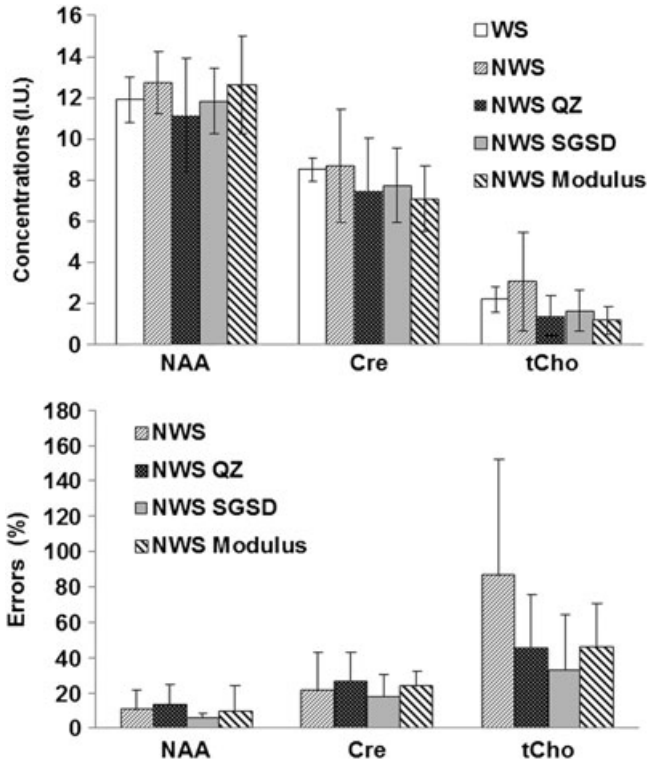

Figure 6. Means and standard deviations of quantified concentrations of *N*-acetylaspartate (NAA), total choline (tCho) and creatine (Cre) from 11 subjects. The quantified results are from water suppression (WS) spectra, non-water suppression (NWS) spectra, NWS spectra corrected using the simultaneous diagonalization method (NWS QZ), NWS spectra corrected using the simultaneously generalized Schur decomposition method (NWS SGSD) and NWS spectra corrected using modulus spectra (NWS Modulus). Results from WS spectra are used as standard. The frequency modulation (FM) sidebands caused overestimation on the metabolic concentrations. (B) Percentage errors in metabolite concentrations using NWS spectra for NAA, tCho, and Cre, compared with values derived from WS spectra. SGSD exhibits the lowest errors in all three metabolites among all NWS spectra.

were implemented using two algorithms, QZ and SGSD, which perform decomposition of a data matrix with reconstruction. The performance of the modulus method and the proposed methods was evaluated using *in vitro* results employing the true reference and *in vivo* results employing WS MRS as the reference. Our *in vitro* results show that the modulus and SGSD methods improve the accuracy of quantification for NAA and Cre. The SGSD method provides superior estimation for tCho (Table 1). Our *in vivo* results show that FM sidebands can be alleviated (Fig. 5), and the spectral peaks can be restored, for superior estimation of concentrations on three major metabolites (Fig. 6). In addition, the SGSD method exhibits superior accuracy to the QZ method and the modulus method. Because the proposed methods are purely post-processing algorithms, substantial changes in pulse sequences or specific experimental design involving additional phantom scans are not required. In general, our algorithm can be fitted to other experimental methods to improve the efficiency of FM sideband suppression.

One of the main advantages of NWS MRS is the potential to perform motion correction and quantification simultaneously (7), with the FM sidebands serving as an additional source of error for spectral quantification. If the profile of FM sidebands can be initially gathered at various locations for follow-up adjustment, in a similar manner to the use of an external reference (12), the efficiency of the removal of FM sidebands can be improved considerably. However, external referencing is feasible only if the scanning condition in the reference scan is similar to that in *in vivo* tissue environments. Otherwise, the FM sidebands may not be fully removed. In the presence of motion, the possible phase alternation during the scan leads to inconsistency between the external reference and scanning condition. A previous study that performed additional calibration with an external reference indicated that, when the power of water was lowered to 10.8% of the original signal, at least 10% errors occurred for quantification in NWS MRS (12). These potential errors caused by external referencing methods in the presence of FM sidebands must be considered for clinical application. In

this case, the use of post-processing approaches for FM sideband removal is favorable.

According to the phantom results, the modulus and SGSD methods outperformed the QZ method in the estimation of absolute and relative concentrations. Although these methods have comparable errors in absolute concentrations of NAA and Cre, overestimation in NAA and underestimation in Cre using the QZ method leads to larger errors in NAA/Cre. Relative quantification using Cre as a reference is generally used in several clinical applications. However, our results indicate that the quantification of Cre is affected by the FM sidebands. Uncertainties remain in the estimation of Cre (Table 1), even after FM sideband reduction. This leads to additional errors when using relative concentrations. Therefore, we suggest that water scaling must be used in NWS MRS for the quantification of concentrations. The extraction of water signals is relatively stable for its intrinsically higher SNR. This makes the water signal suitable as a reference signal.

A property of SGSD and QZ is that the estimation of poles, especially during the extraction of the FM contribution, is sensitive to noise disturbance, linewidth and baseline distortion. Therefore, these factors can influence the performance of SGSD and QZ. Although the simulation shows that the performance of the SGSD method is close to the theoretical limits set by CRLB (Fig. 3D), the *in vivo* results generally digress from ideal conditions because of field inhomogeneity, which can be particularly prominent in intricate tissues. A previous study has indicated that the efficiency of the reduction of FM sidebands is influenced by the linewidth of artifacts (31). It is usually difficult to accurately extract FM sidebands with broad linewidths. This occurred for the multiplets of Glx (Glu + Gln) and mI in short-TE spectra, the quantification of which was not improved using FM sideband correction. Another consideration of these methods is the length of data included for calculation. A larger data length improves the stability, as demonstrated by the simulation (Fig. 3). Methods to enhance computation stability have been proposed, such as the alternating least-square method (23,24) or other nonlinear methods (34); however, these methods are outside the scope of this study.

The computational complexity of SVD is $O(n^3)$. This implies that the operation of SVD is time consuming when the matrix size increases. The computation for SGSD is more complex. Moreover, the matrix multiplication of the associated orthogonal transformation may also cost computational time. In our study, the entire computational time was within 1 min when the operation was performed on a regular PC (2.67-GHz CPU with 2 GB RAM) for a data length of 128 points. The computational time can be further improved by applying numerical methods, such as nonlinear orthogonal reduction (23,24), or by using parallel computing with modern graphical processing units.

A comparison of the SGSD and modulus methods revealed that SGSD shows superior estimation of tCho to the modulus method in *in vitro* results (Table 1) and fewer errors in *in vivo* results (Fig. 6). However, the modulus method has a number of advantages. First, the implementation of the modulus method is relatively simple and the computational complexity is low compared with the SGSD method. Second, although SGSD and QZ estimate the possible contribution of FM sidebands and subtract them, the modulus method can theoretically cancel the FM sidebands completely using the anti-phase property of FM sidebands. However, the trade-off is SNR reduction, linewidth alteration and contamination from spectral lines from the downfield range regarding the water signal (20). This may be the main source of errors in the modulus method.

In summary, the SGSD method, with its implications on signal processing problems (26), is useful to reduce FM sidebands of NWS MRS. Post-processing methods are valuable because they can be used directly to process the spectra acquired under various experimental conditions. In addition, information such as phase and magnitude, extracted by the SGSD method, can be useful for other applications. For example, simultaneous estimation of phase and magnitude in the time domain from each coil is helpful for data combination involving the use of multiple coils (13,32). The main disadvantage of the SGSD method is that, although it can be implemented at short TE, only the quantification of the three major metabolites is improved; the estimation of the coupled resonances is not improved. The performances of the proposed post-processing methods are limited if the FM sidebands are not fully accordant with the assumed signal model. Therefore, the further development of the post-processing method for superior efficiency and flexibility is crucial, and is under further investigation.

CONCLUSIONS

This study demonstrated that the proposed QZ and SGSD algorithms can reduce water-related FM sideband artifacts in NWS MRS, which makes NWS MRS more practical in general applications. The performance of these methods was examined using computer simulation, *in vitro* and *in vivo* studies. Our results showed that SGSD has superior accuracy for the reduction of FM sidebands. This algorithm can be combined with any experimental method to achieve superior efficiency for the suppression of FM sideband artifacts.

Acknowledgements

Funding from the National Science Council (NSC98-2320-B-182-003-MY2, NSC98-2221-E-002-095-MY3) is gratefully acknowledged.

REFERENCES

1. Seppenwoolde JH, van Zijtveld M, Bakker CJ. Spectral characterization of local magnetic field inhomogeneities. Phys. Med. Biol. 2005; 50(2): 361–372.
2. Spielman D, Webb P, Macovski A. Water referencing for spectroscopic imaging. Magn. Reson. Med. 1989; 12(1): 38–49.
3. Webb P, Spielman D, Macovski A. Inhomogeneity correction for in vivo spectroscopy by high-resolution water referencing. Magn. Reson. Med. 1992; 23(1): 1–11.
4. Leibfritz D, Dreher W. Magnetization transfer MRS. NMR Biomed. 2001; 14(2): 65–76.
5. Gabr RE, Sathyanarayana S, Schar M, Weiss RG, Bottomley PA. On restoring motion-induced signal loss in single-voxel magnetic resonance spectra. Magn. Reson. Med. 2006; 56(4): 754–760.
6. Katz-Brull R, Lenkinski RE. Frame-by-frame PRESS ^{1}H-MRS of the brain at 3 T: the effects of physiological motion. Magn. Reson. Med. 2004; 51(1): 184–187.
7. Lin JM, Tsai SY, Liu HS, Chung HW, Mulkern RV, Cheng CM, Yeh TC, Chen NK. Quantification of non-water-suppressed MR spectra with correction for motion-induced signal reduction. Magn. Reson. Med. 2009; 62(6): 1394–1403.
8. Prakash V, Stainsby JA, Satkunasingham J, Craig T, Catton C, Chan P, Dawson L, Hensel J, Jaffray D, Milosevic M, Nichol A, Sussman MS, Lockwood G, Menard C. Validation of supervised automated algorithm for fast quantitative evaluation of organ motion on magnetic resonance imaging. Int. J. Radiat. Oncol. Biol. Phys. 2008; 71(4): 1253–1260.

9. Star-Lack JM, Adalsteinsson E, Gold GE, Ikeda DM, Spielman DM. Motion correction and lipid suppression for ^{1}H magnetic resonance spectroscopy. Magn. Reson. Med. 2000; 43(3): 325–330.
10. Thiel T, Czisch M, Elbel GK, Hennig J. Phase coherent averaging in magnetic resonance spectroscopy using interleaved navigator scans: compensation of motion artifacts and magnetic field instabilities. Magn. Reson. Med. 2002; 47(6): 1077–1082.
11. Barker PB, Soher BJ, Blackband SJ, Chatham JC, Mathews VP, Bryan RN. Quantitation of proton NMR spectra of the human brain using tissue water as an internal concentration reference. NMR Biomed. 1993; 6(1): 89–94.
12. Özdemir MS, Deene YD, Fiermans E, Lemahieu I. Quantitative proton magnetic resonance spectroscopy without water suppression. J. Instrum. 2009; 4(06): P06014.
13. Dong Z, Peterson B. The rapid and automatic combination of proton MRSI data using multi-channel coils without water suppression. Magn. Reson. Imaging, 2007; 25(8): 1148–1154.
14. Clayton DB, Elliott MA, Lenkinski RE. In vivo proton spectroscopy without solvent suppression. Conc. Magn. Res. 2001; 13(4): 260–275.
15. Dong Z, Dreher W, Leibfritz D. Toward quantitative short-echo-time in vivo proton MR spectroscopy without water suppression. Magn. Reson. Med. 2006; 55(6): 1441–1446.
16. Serrai H, Senhadji L, Clayton DB, Zuo C, Lenkinski RE. Water modeled signal removal and data quantification in localized MR spectroscopy using a time-scale postacquistion method. J. Magn. Reson. 2001; 149(1): 45–51.
17. van Der Veen JW, Weinberger DR, Tedeschi G, Frank JA, Duyn JH. Proton MR spectroscopic imaging without water suppression. Radiology, 2000; 217(1): 296–300.
18. Clayton DB, Elliott MA, Leigh JS, Lenkinski RE. ^{1}H spectroscopy without solvent suppression: characterization of signal modulations at short echo times. J. Magn. Reson. 2001; 153(2): 203–209.
19. Lathi BP. *Communication Systems*. Wiley: New York; 1968.
20. Dong Z, Dreher W, Leibfritz D. Experimental method to eliminate frequency modulation sidebands in localized in vivo ^{1}H MR spectra acquired without water suppression. Magn. Reson. Med. 2004; 51(3): 602–606.
21. Hurd RE, Gurr D, Sailasuta N. Proton spectroscopy without water suppression: the oversampled J-resolved experiment. Magn. Reson. Med. 1998; 40(3): 343–347.
22. Serrai H, Clayton DB, Senhadji L, Zuo C, Lenkinski RE. Localized proton spectroscopy without water suppression: removal of gradient induced frequency modulations by modulus signal selection. J. Magn. Reson. 2002; 154(1): 53–59.
23. Stegeman A Using the simultaneous generalized Schur decomposition as a Candecomp/Parafac algorithm for ill-conditioned data. J. Chemometrics, 2009; 23(7–8): 385–392.
24. Kiers H, ten Berge J. Alternating least squares algorithms for simultaneous components analysis with equal component weight matrices in two or more populations. Psychometrika, 1989; 54(3): 467–473.
25. Delathauwer L, Castaing J. Tensor-based techniques for the blind separation of DS–CDMA signals. Signal Process. 2007; 87(2): 322–336.
26. van der Veen AJ, Paulraj A. An analytical constant modulus algorithm. IEEE Trans. Signal Processing, 1996; 44(5): 1136–1155.
27. Vanhuffel S, Chen H, Decanniere C, Vanhecke P. Algorithm for time-domain NMR data fitting based on total least squares. J. Magn. Reson., Ser. A, 1994; 110(2): 228–237.
28. Lin Y-Y, Hodgkinson P, Ernst M, Pines A. A novel detection-estimation scheme for noisy NMR signals: applications to delayed acquisition data. J. Magn. Reson. 1997; 128(1): 30–41.
29. Mandelshtam V, Taylor H. Harmonic inversion of time signals and its applications. J. Chem. Phys. 1997; 107(17): 6756–6769.
30. Hu H, Van QN, Mandelshtam VA, Shaka AJ. Reference deconvolution, phase correction, and line listing of NMR spectra by the 1D filter diagonalization method. J. Magn. Reson. 1998; 134(1): 76–87.
31. Steedly WM, Moses RL. The Cramer–Rao bound for pole and amplitude coefficient estimates of damped exponential signals in noise. IEEE Trans. Signal Processing, 1993; 41(3): 1305–1318.
32. Brown MA. Time-domain combination of MR spectroscopy data acquired using phased-array coils. Magn. Reson. Med. 2004; 52(5): 1207–1213.
33. Ratiney H, Coenradie Y, Cavassila S, van Ormondt D, Graveron-Demilly D. Time-domain quantitation of ^{1}H short echo-time signals: background accommodation. MAGMA, 2004; 16(6): 284–296.
34. Oseledets IV, Savostyanov DV, Tyrtyshnikov EE. Fast simultaneous orthogonal reduction to triangular matrices. SIAM J. Matrix Anal. Appl. 2009; 31(2): 316–330.
35. Golub GH. *Matrix Computations*. Johns Hopkins University Press: Baltimore, MD; 1996.
36. Mandelshtam VA, Taylor HS, Shaka AJ. Application of the filter diagonalization method to one- and two-dimensional NMR spectra. J. Magn. Reson. 1998; 133(2): 304–312.
37. De Lathauwer L, De Moor B, Vandewalle J. Computation of the canonical decomposition by means of a simultaneous generalized Schur decomposition. SIAM J. Matrix Anal. Appl. 2004; 26(2): 295.

APPENDIX

SOLVING GEP WITH QZ

The problem can be solved by introducing U_0 and U_1 from the time-domain data:

$$U_0 = \begin{bmatrix} \hat{s}(0) & \hat{s}(1) & \cdots & \hat{s}(M-1) \\ \hat{s}(1) & \hat{s}(2) & \cdots & \hat{s}(M) \\ \vdots & \vdots & \ddots & \vdots \\ \hat{s}(M-1) & \hat{s}(M) & \cdots & \hat{s}(2M-2) \end{bmatrix} = V \times Diag\{A_1, A_2, \ldots, A_K, 0, \ldots, 0\} \times V^T \quad [A1]$$

$$U_1 = \begin{bmatrix} \hat{s}(1) & \hat{s}(2) & \cdots & \hat{s}(M) \\ \hat{s}(2) & \hat{s}(3) & \cdots & \hat{s}(M+1) \\ \vdots & \vdots & \ddots & \vdots \\ \hat{s}(M) & \hat{s}(M+1) & \cdots & \hat{s}(2M-1) \end{bmatrix} = V \times Diag\{\lambda_1, \lambda_2, \ldots, \lambda_K, 0, \ldots, 0\} \times Diag\{A_1, A_2, \ldots, A_K, 0, \ldots, 0\} \times V^T \quad [A2]$$

where λ_i, $i = 1, 2\ldots, k$, are distinct eigenvalues of each component, A_i are amplitudes, M is the dimension of the matrices, which must be larger than the number of components, and V is the Vandermonde matrices of the poles:

$$V = \begin{bmatrix} 1 & 1 & \cdots & 1 \\ \lambda_1 & \lambda_2 & \cdots & \lambda_K \\ \vdots & \vdots & \ddots & \vdots \\ {\lambda_1}^{M-1} & {\lambda_2}^{M-1} & \cdots & {\lambda_K}^{M-1} \end{bmatrix} | 0 \quad [A3]$$

The time-domain signals are arranged as Hankel matrices (in the form of Toeplitz matrices). Consequently, the poles embedded inside Equation [A2] are solved using the following generalized eigen equation:

$$U_1 E - \lambda U_0 E = 0 \quad [A4]$$

where E contains the eigenvectors for individual eigenvalues in distinct columns. λ are generalized eigenvalues. The solutions towards poles and amplitudes are embedded in the structure of the matrices in Equations [A1] and [A2]. An established method is the QZ algorithm (35), through which both U_0 and U_1 are triangularized with a pair of orthogonal matrices, Q and Z:

$$\begin{aligned} U_{0t} &= \mathrm{Q} U_0 \mathrm{Z} \\ U_{1t} &= Q U_1 \mathrm{Z} \end{aligned} \quad [A5]$$

The ratios of the diagonal elements of U_{0t} and U_{1t}, that is, b_{ii} and a_{ii}, generate the generalized eigenvalues:

$$\lambda_i = a_{ii}/b_{ii}, \qquad i = 1, \ldots, M \quad [A6]$$

where the small diagonal elements are attributed to zero space in Equations [A1] and [A2].

NMR IN BIOMEDICINE

Although matrix inversion does not occur, the QZ method provides a reasonable estimator for an ill-conditioned problem, in which the eigenvalues are represented as ratios. Another advantage of GEP is that amplitudes for each component are solely determined from the eigenvectors. Without another least-square problem, the amplitudes are (29,30,36):

$$A_i = (U_{0t}E_i)^2 \qquad [A7]$$

SGSD AS AN EXTENSION OF QZ

The SGSD method has been developed during recent years (23,26,37), and simultaneously triangularizes three or more matrices. Because SGSD is an extension of QZ, the simplest implementation of SGSD is called the extended QZ method, which adds additional orthogonal transformation to the whole set of matrices.

We generalized the two-matrix case to multiple matrices U_r. Starting from the QZ method (Q and Z are obtained from the first two matrices) of two matrices:

$$U_{rt} = QU_rZ, \qquad r = 1, \ldots, R \qquad [A8]$$

Because the QZ algorithm derived an approximation in Equation [A8], the set of matrices was quasi-triangularized, which indicates that the off-diagonal elements are close to zero. However, the solution of QZ is only an approximation for the other matrices, because round-off errors and noise may influence the accuracy. To enhance the reliability, we constructed a series of new Qs and Zs from the whole set of matrices. This starts by constructing another Householder matrix H_1 from the first columns of U_r, as is computed from the left singular vector of the matrix. The first columns of U_r are concurrently triangularized, and the second columns are subsequently calculated. Finally, the new U_r are transformed using Q step:

$$\begin{aligned} U_{rt} &= Q_M \ldots Q_2 Q_1 U_r, \qquad r = 1, \ldots, R \\ &= \begin{bmatrix} I_{(M-1)} & 0 \\ 0 & H_M \\ & 1 \times 1 \end{bmatrix} \begin{bmatrix} I_{(M-2)} & 0 \\ 0 & H_{M-1} \\ & 2 \times 2 \end{bmatrix} \cdots \\ &\quad \begin{bmatrix} 1 & 0 \\ 0 & H_2 \\ & (M-1) \times (M-1) \end{bmatrix} \begin{bmatrix} H_1 \\ M \times M \end{bmatrix} U_r \end{aligned} \qquad [A9]$$

Similarly, the additional Z transforms are obtained from the last rows of each U_r, whereas the right singular vector V_1 with reverse order of singular values constructs the first Z_1. After the first row has been transformed by Z_1, the second rows may be transformed using the same procedure. The following denotes transformation of U_r with Z steps:

$$\begin{aligned} U_{rt} &= U_r Z_1 \ldots Z_{M-1} Z_M, \qquad r = 1, \ldots, R \\ &= U_r \begin{bmatrix} V_1 \\ M \times M \end{bmatrix} \begin{bmatrix} V_2 & 0 \\ (M-1) \times (M-1) & \\ 0 & 1 \end{bmatrix} \cdots \\ &\quad \begin{bmatrix} V_{M-1} & 0 \\ 2 \times 2 & \\ 0 & I_{(M-2)} \end{bmatrix} \begin{bmatrix} V_M & 0 \\ 1 \times 1 & \\ 0 & I_{(M-1)} \end{bmatrix} \end{aligned} \qquad [A10]$$

Subsequently, the Z step must be applied to update the eigenvectors:

$$E_t = EZ \qquad [A11]$$

